Journal of Photochemistry and Photobiology A: Chemistry 210 (2010) 61–68

Contents lists available at ScienceDirect

Journal of Photochemistry and Photobiology A: Chemistry

journal homepage: www.elsevier.com/locate/jphotochem

TiO_2 photocatalytic degradation of phenylarsonic acid

Shan Zheng, Yong Cai, Kevin E. O'Shea *

Department of Chemistry and Biochemistry, Florida International University, Miami, FL 33199, United States

ARTICLE INFO

Article history:
Received 7 August 2009
Received in revised form
25 November 2009
Accepted 8 December 2009
Available online 16 December 2009

Keywords:
Titanium dioxide
Heterogeneous photocatalysis
Phenylarsenic acid
Degradation

ABSTRACT

Phenyl substituted arsenic compounds are widely used as feed additives in the poultry industry and have become a serious environmental concern. We have demonstrated that phenylarsonic acid (PA) is readily degraded by TiO_2 photocatalysis. Application of the Langmuir–Hinshelwood kinetic model for the initial stages of the TiO_2 photocatalysis of PA yields an apparent rate constant (k_r) of 2.8 μmol/L min and the pseudo-equilibrium constant (K) for PA is 34 L/mmol. The pH of the solution influences the adsorption and photocatalytic degradation of PA due to the surface charge of TiO_2 photocatalyst and speciation of PA. Phenol, catechol and hydroquinone are observed as the predominant products during the degradation. The roles of reactive oxygen species, $^{\bullet}OH$, $^1O_2$, $O_2^{-\bullet}$ and h_{VB}^+ were probed by adding appropriate scavengers to the reaction medium and the results suggest that $^{\bullet}OH$ plays a major role in the degradation of PA. By-product studies indicate the surface of the catalyst plays a key role in the formation of the primary products and the subsequent oxidation pathways leading to the mineralization to inorganic arsenic. TiO_2 photocatalysis results in the rapid destruction of PA and may be attractive for the remediation of a variety of organoarsenic compounds.

1. Introduction

Inorganic arsenic species As(III) and As(V) are naturally occurring toxic substances, which threaten the health of millions of people because of the consumption of water contaminated with inorganic arsenic [1]. Due to its high toxicity in humans, the U.S. Environmental Protection Agency (EPA) has lowered the maximum contaminant level of inorganic arsenic in drinking water from 50 to 10 μg/L [2]. While the treatment and removal of As(III) and As(V) from drinking water have received extensive attention [3–5], the wide spread use and environmental threat of organoarsenic species have received much less attention.

Organoarsenic compounds typically exist in the pentavalent oxidation state and have been introduced into the environment through agricultural applications [2,6]. Methylated arsenicals are widely used as herbicides for cotton farming and golf course maintenance with the application of 5000 tons/year worldwide [7]. Phenylated arsenic compounds including 4-hydroxy-3-nitrophenylarsenic acid (roxarsone), 4-aminophenylarsenic acid (*p*-arsanilic acid), etc. [8] are commonly utilized in the broiler poultry industry as feed additives to control cecalcoccidiosis. Initially these compounds were believed to be nontoxic to domestic livestock, and excreted unchanged following ingestion by the animals [9]. Arsenic contaminated poultry litter, is sold and distributed as fertilizer, leading to large areas of arsenic contaminated soils. The PA feed additives were reported to be inert in the environment, however recent reports indicate these nontoxic organoarsenic compounds may be converted into more mobile and toxic inorganic arsenic species [10–13]. Biotransformation also produces toxic inorganic arsenic compounds from organoarsenicals [14]. The biological and environmental transformations of organoarsenicals can lead to the contamination of local water supplies with a complex mixture of arsenic containing substrates.

TiO_2 photocatalytic oxidation, an advanced oxidation process (AOP), is a promising technology for environmental purification. TiO_2 is the most extensively used semiconductor photocatalyst because of its photocatalytic activity, chemical stability, nontoxicity and low cost. When TiO_2 is subjected to UV light ($\lambda > 385$ nm), an electron/hole pair (e_{CB}^-/h_{VB}^+) is generated. Photocatalytic reactions take place primarily on the surface of TiO_2, where the photogenerated electrons and holes are trapped [15]. The electron reacts with adsorbed oxygen, yielding superoxide radical ($O_2^{-\bullet}$), which can act as an oxidant or reductant. In the aqueous media, the hole typically reacts with adsorbed H_2O, hydroxide or surface titanol groups (–TiOH) to produce hydroxyl radical ($^{\bullet}OH_{abs}$), which is a powerful oxidant [16]. The reactive species (i.e., h_{VB}^+, e_{CB}^-, $^{\bullet}OH$, $O_2^{-\bullet}$, $^{\bullet}O_2H$, H_2O_2, $^1O_2$, etc.) generated during TiO_2 photocatalysis can lead to the destruction of problematic pollutants.

A number of different oxidative methods have been employed to convert arsenite to arsenate, including H_2O_2, UV/H_2O_2, oxygen and ozone (O_3), MnO_2, Fenton's reagent (Fe(II)/H_2O_2), and

* Corresponding author. Tel.: +1 305 348 3968; fax: +1 305 348 3772.
E-mail address: osheak@fiu.edu (K.E. O'Shea).

1010-6030/$ – see front matter © 2009 Elsevier B.V. All rights reserved.
doi:10.1016/j.jphotochem.2009.12.004

UV/Fe(III), however each method has specific limitations and disadvantages [17]. TiO_2 photocatalysis leads to the remediation of pollutants with UV irradiation under mild conditions [18,19]. The TiO_2 photocatalytic oxidation (PCO) of As(III) to As(V) occurs in an adsorbed state and via a rapid process [20], but recent reports dispute the roles of $^{\bullet}OH$, $O_2^{-\bullet}$ and hole during TiO_2 photocatalysis of As(III) [17,21–25]. TiO_2 is a powerful adsorbent for arsenic species, and thus TiO_2 photocatalysis has attracted tremendous interest for treatment of toxic arsenic species [26,27]. Methylated arsenic species, monomethyl arsonic acid (MMA) and dimethyl arsonic acid (DMA) are oxidized by $^{\bullet}OH$ and mineralized to As(V) upon TiO_2 photocatalysis [28]. The TiO_2 photocatalytic oxidation of inorganic arsenic, As(III) involves direct oxidation of the arsenic atom to yield As(IV) which is rapidly converted to arsenate, As(V) [29]. However, TiO_2 photocatalysis of methylated arsenic species, appears to involve hydrogen abstraction pathways (leading to the oxidation of the carbon atom) as the initial oxidation step to yield a carbon centered radical which can undergo a series of oxidative processes leading to inorganic arsenate. Although recent studies demonstrated that PA is very reactive toward radiolytically generated hydroxyl and sulfate radicals in homogenous solution [30], to the best of our knowledge, TiO_2 photocatalysis of phenylated arsenic species has not been reported in the literature. Extensive comparisons have been made between hydroxyl radical reactivities generated via radiolysis (homogeneous conditions) and via TiO_2 photocatalysis (heterogeneous conditions). Unlike radiolysis, which leads to clean generation of hydroxyl radicals, TiO_2 photocatalysis leads to the formation of several potential oxidants at surface of the photocatalyst. During TiO_2 photocatalysis reactions occur at or very near the surface and the observed reaction pathways can be dramatically influenced by adsorption properties of the reactants as well as the reactivity of the reactant in the adsorbed state. With this in mind we chose to conduct for the first time detailed by-products and kinetic studies in the TiO_2 photocatalytic degradation of PA to better understand the role of the surface in the TiO_2 photocatalysis of PA. The mineralization of PA to As(V) is rapid and appears to occur via surface adsorbed $^{\bullet}OH$. Solution pH influences the degradation and the TiO_2 surface influences the partitioning of the reaction pathways.

2. Experiments

2.1. Materials

Analytical-reagent grade chemicals were used as received. Millipore filtered water (18 MΩ cm) was used to prepare all solutions. Phenylarsonic acid (PA), 2-hydroxylphenylarsonic acid (2-OH-PA) and 4-hydroxylphenylarsonic acid (4-OH-PA) were purchased from Avocado were used as authentic samples for chromatographic comparison. Titanium dioxide (Degussa P25), a mixture of 80% anatase and 20% rutile with an average surface area of 50 m^2/g, was used as the photocatalyst.

2.2. Sample preparation

TiO_2 concentration employed for our studies was 0.1 g/L and $[PA]_0$ = 38 μmol/L unless otherwise stated. In general 100 mL of solution was prepared and the resulting TiO_2 suspension was dispersed using an ultrasonic cleaning bath for 15 min. The solution was magnetically stirred in the dark. One hour of stirring in the dark was sufficient to reach adsorption equilibrium prior to irradiation. The suspension was transferred to pyrex cylindrical reactor (12 × 1 in., 160 mL capacity, with a vented Teflon screw top). The solution was saturated with the desired gas by purging (air, oxygen or argon) for 15 min prior to irradiation and continued until the end of the reaction. The majority of experiments were performed at air-saturated conditions. Irradiation of suspension was conducted in a Rayonet photochemical reactor (Southern New England Ultra Violet Company, www.rayonet.org), model RPR-100, equipped with a cooling fan and 15 phosphor-coated low-pressure mercury lamps. Pyrex cylindrical reaction vessel with the suspension was clamped in the center of the photochemical reactor. The lamps had a spectral energy distribution with a maximum intensity at λ = 350 nm, and yielding an incident light intensity of $5.2 \pm 0.1 \times 106$ photon/s/cm^3. Ferrioxalate actinometry was used to measure the light intensity [31]. Five milliliter samples were periodically withdrawn, filtered through a 0.45 μm filter, and analyzed by HPLC-ICP-MS.

2.3. Analysis

Total arsenic concentrations were determined by inductively coupled plasma mass spectroscopy (ICP-MS, HP 4500). The plasma and auxiliary gas flow rate for the ICP-MS were maintained at 15.4 and 1.0 L/min, respectively. Arsenic speciation was determined by continuous high-performance liquid chromatography (HPLC) coupled with ICP-MS detection. An anion-exchange column, Dionex AS 7 (250 mm × 4 mm, 5 μm particle size) was used for the separation of arsenic species. The mobile phase was HNO_3 aqueous solution (pH 2.0), and the flow rate was 0.5 mL/min. On the basis of LC-ICP-MS data and correlation of the chromatographic behavior of the products to authentic compounds, the identity of the products appearing in the chromatogram were was assigned as follows; peak 1 = As(III) (180 s), peak 2 = PA (380 s), peak 3 = 2-hydroxylphenylarsonic acid (460 s), peak 4 = 4-hydroxylphenylarsonic acid (520 s), peak 5 = dihydroxyl phenylarsonic acid (600 s), peak 6 = As(V) (730 s). Although dihydroxyl-substituted isomer is not commercially available for confirmation, it was previously assigned based on the MS data [30].

The analysis for phenolic compounds was conducted using GC (HP 5890 Series II). The aqueous reaction solutions were extracted by methylene chloride (HPLC grade) and subsequently analyzed on GC. The injection port temperature was maintained at 250 °C and the injection volume was 1 μL. The column was DB-5 (30 m × 0.53 mm), and the film thickness was 0.25 μm. The carrier gas was helium with 99.9999% purity at a constant flow rate of 2.7 mL/min, and the temperature of the FID detector was 320 °C. The initial oven temperature was 40 °C for 3 min, ramped at 5 °C/min to 200 °C. Authentic standards were used to confirm the chromatographic behavior of the products.

3. Results and discussions

3.1. PA adsorption on TiO_2 photocatalyst (dark)

In order to better understand the adsorption process and its role on the TiO_2 photocatalytic degradation process, the adsorption of PA in dark was studied as a function of initial PA concentration without adjusting solution pH. The concentration of PA varied from 5 to 100 μmol/L at a constant TiO_2 concentration of 0.1 g/L. Our initial studies established that the adsorption equilibrium was maintained by stirring the dispersion in dark for 60 min.

Langmuir adsorption isotherms, which are often used to describe the heterogeneous adsorption process [32], were employed to assess the PA adsorption capacity of TiO_2. Unique adsorption sites, monolayer adsorption, and no interaction between the adsorption sites are the underlying assumptions used in deriving the Langmuir isotherm. Langmuir adsorption isotherm

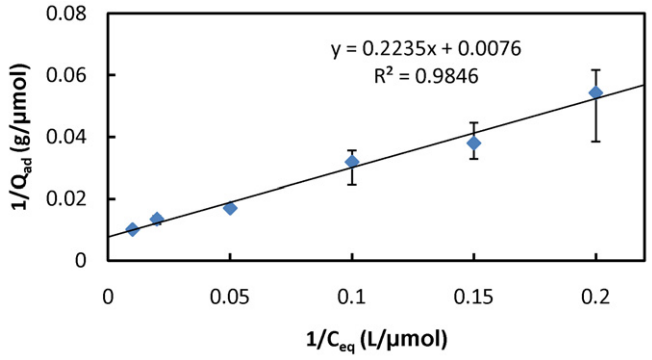

Fig. 1. Langmuir isotherm dark adsorption of PA on TiO_2 photocatalyst, $[TiO_2] = 0.1$ g/L. Error bars represent one standard deviation based on triplicate experiments.

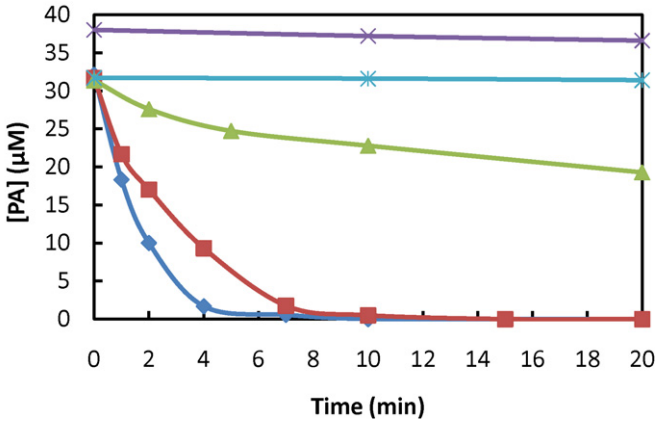

Fig. 2. Time profiles of PA degradation in the TiO_2 suspension under various reaction conditions. $[PA]_0 = 38$ μmol/L; $[TiO_2] = 0.1$ g/L; $\lambda = 350$ nm (✕ w/o TiO_2, ✳ w/o UV, ▲ Ar-saturated, ■ air-saturated, and ◆ O_2-saturated).

can be described by equation:

$$Q_{ad} = Q_{sat}\frac{K_{ad}C_{eq}}{1 + K_{ad}C_{eq}} \quad (1)$$

where Q_{ad} is the specific adsorbed quantity of a model compound and C_{eq} is the initial concentration; Q_{sat} is the saturation (maximum) adsorption capacity and K_{ad} is the adsorption constant.

The dark adsorption of PA is nicely described by Langmuir adsorption isotherm with coefficient $R^2 = 0.9844$, shown in Fig. 1. Q_{sat} is 123 ± 10 μmol/g for PA adsorption on TiO_2 photocatalyst. Xu et al. [28] reported Q_{sat} for MMA and DMA of 86 and 37 μmol/g respectively. Similar values for PA and MMA are consistent with their analogous structures. Based on the estimated density of surface hydroxyl groups of 4.8 OH/(nm)^2 present on Degussa P25TiO_2 [33], the maximum adsorption capacity of PA on the TiO_2 surface is 400 μmol/g assuming no steric constraints and a bidentate adsorption mode. The maximum adsorbed concentration observed under our experimental conditions corresponds to $30 \pm 3\%$ monolayer coverage for PA. We consider 30% surface coverage to be relatively high given the theoretical (improbable) assumption that every surface hydroxyl group can contribute to PA adsorption. In addition, the catalyst undergoes rapid agglomeration that significantly reduces the effective surface area and number of available adsorption sites [34]. The equilibrium, K_{ad} between the adsorption and desorption of PA on the surface of TiO_2 is 0.0367 L/μmol.

3.2. TiO_2 photocatalytic degradation of PA

TiO_2 photocatalysis was carried out as an aqueous suspension of TiO_2 (0.1 g/L) and PA at room temperature. The solution was purged with air, oxygen or argon prior to the irradiation. The solution (100 mL) was irradiated in a Rayonet reactor with 15 phosphor-coated low-pressure mercury lamps emitting UV light (350 nm). The results are illustrated in Fig. 2. Degradation of PA in the absence of TiO_2 or UV is negligible. The 10–20% decrease in PA concentration without UV irradiation is due to PA adsorption onto the TiO_2 surface. The degradation is also relatively slow under argon-saturated conditions. Under our experimental conditions, TiO_2, dissolved oxygen and UV light are required for effective degradation of PA.

While TiO_2 photocatalysis involves heterogeneous processes, the initial degradation often follows 1st order kinetics [28,30]. With this in mind, plots of $\ln(C_0/C_t)$ vs. time were constructed for TiO_2 photocatalysis of PA under Ar-, air- and O_2-saturated conditions. The 1st order PA degradation plots exhibit linear relationships and $k_{Ar} = 0.04 \pm 0.01$ min^{-1}, $k_{air} = 0.36 \pm 0.04$ min^{-1}, and $k_{O_2} = 0.68 \pm 0.01$ min^{-1}.

3.3. Heterogeneous kinetics

The Langmuir–Hinshelwood (L–H) model is often applied to obtain kinetic parameters for reactions occurring at a solid–liquid interface during photocatalysis [35]. Application of the L–H model enables the observed kinetics to be separated into reactivity and adsorption components. One of the simplest representations of the L–H model is given by:

$$r_0 = \frac{dC}{dt} = \frac{k_r K C_0}{1 + K C_0} \quad (2)$$

where r_0 is the initial rate (observed) of disappearance of substrate, C_0 is the initial substrate concentration, k_r is a reactivity coefficient relating to oxidation events at the catalyst's surface, and K is pseudo-equilibrium constant related to surface adsorption [36]. The apparent kinetic parameters k_r and K can be obtained from a plot of $1/r_0$ vs. $1/C_0$.

$$\frac{1}{r_0} = \frac{1}{k_r K C_0} + \frac{1}{k_r} \quad (3)$$

To minimize interference from by-products, the L–H model is generally applied to the first 10–20% of reaction and low initial concentrations are employed to minimize the potential for interference from multilayer adsorption. The photocatalytic experiments were performed over a range of initial PA concentrations (10–100 μmol/L) and a constant TiO_2 concentration of 0.1 g/L under uniform photon flux (light intensity: $1.12 \pm 0.1 \times 10^6$ photon/s/cm^3).

The L–H kinetic parameters were determined from the slope and intercept of the linear fit of the $1/r_0$ vs. $1/C_0$ (Fig. 3). Under our experiment conditions, k_r is 2.8 μmol/L min and K is 34 L/mmol for PA. The L–H kinetic parameters for MMA under similar conditions were $k_r = 1.8$ μmol/L min and $K = 33$ L/mmol [28]. MMA and PA have analogous structures except MMA has a single methyl group and PA has a single phenyl group neither of which is expected to have a significant influence on the adsorption. The L–H equilibrium constants of MMA and PA are essentially the same, however the reactivity, k_r, of MMA is significantly lower than PA. The absolute hydroxyl radical rate constants in homogenous media for •OH with MMA and PA are $\sim 10^8$ and $\sim 10^{10}$ M^{-1} s^{-1} respectively [30]. While the TiO_2 photocatalytic degradation of MMA and PA may both involve •OH, the difference in observed reactivity implies different reaction pathways are involved for MMA and PA. The pathway to MMA likely involves hydroxyl radical abstraction of hydrogen from the methyl group of MMA [37], while in the case of PA hydroxyl radical likely reacts via addition to the aromatic ring (typically 10–100 times

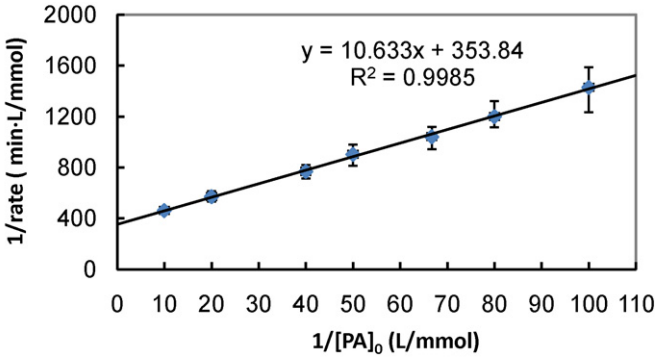

Fig. 3. Langmuir–Hinshelwood plot of TiO_2 photocatalytic degradation of PA. $[PA]_0 = 38\ \mu mol/L$; $[TiO_2] = 0.1\ g/L$; air-saturated; $\lambda = 350\ nm$. Error bars represent one standard deviation based on triplicate experiments.

faster than the hydrogen abstraction pathway). The final oxidation product of PA is arsenate. Arsenate is strongly adsorbed onto the TiO_2 surface [20] and may adversely influence the adsorption and degradation kinetics at high initial PA concentrations.

3.4. pH effects

TiO_2 photocatalysis of PA was conducted under acidic, neutral and basic pH conditions. The solution pH was adjusted from 3 to 11 using 0.1 M HNO_3 and 0.1 M NaOH prior to the irradiation. PA exhibits highest adsorption at acidic and neutral pH. PA adsorption decreases dramatically under basic conditions indicative of repulsion of the negative charges on PA and the TiO_2 surface under basic conditions. TiO_2 has a point of zero charge in solution pH 6.8. The results of the adsorption of PA as a function of solution pH are summarized in Fig. 4. Under acidic conditions, the positive charge of the TiO_2 surface increases as the pH decreases; above pH 6.8, the negative charge at the surface of TiO_2 increases with the increasing pH. The pKa values of PA are 3.8 and 8.5, and PA exists predominantly as a mono-anion between pH 3.8 and 8.5, and as di-anion at pH > 8.5. PA is strongly adsorbed on the surface of TiO_2 under acidic conditions because of the electrostatic attraction of the negative change associated with PA and the positive charge associated with the TiO_2. Under basic conditions PA and TiO_2 process negative charges which will create electrostatic repulsion and reduce the level of surface adsorption. Such pH effects have been observed for a variety of ionizable substrates [28,38].

The L–H behavior and the observed pH effects indicate the transformations of PA, during TiO_2 photocatalysis, involve reactions at or very near the surface and thus are strongly dependent on the interaction between substrate and TiO_2 [39]. We also evaluated the

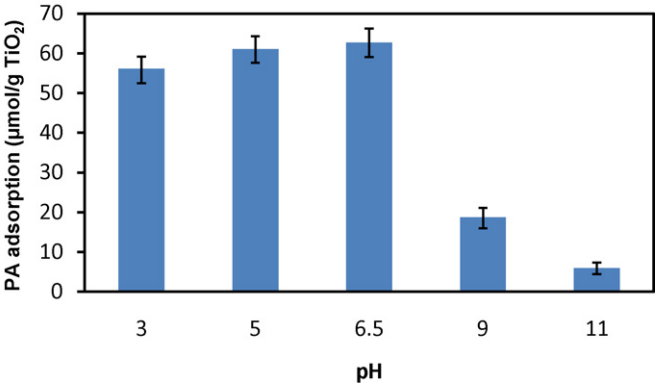

Fig. 4. pH effects on PA adsorption on TiO_2 photocatalyst, $[PA]_0 = 38\ \mu mol/L$, $[TiO_2] = 0.1\ g/L$. Error bars represent one standard deviation based on triplicate experiments.

Table 1
1st order kinetics parameters for TiO_2 photocatalytic degradation of PA.

Saturation gas[a]	pH	k (min^{-1})[b]	$\tau_{1/2}$ (min)	R^2
Argon	6.5	0.04 ± 0.01	17.3	0.96
Air	6.5	0.36 ± 0.04	1.9	0.97
Oxygen	6.5	0.68 ± 0.10	1.0	0.98
Air	3	0.33 ± 0.03	2.1	0.99
Air	5	0.33 ± 0.03	2.1	0.99
Air	9	0.44 ± 0.05	1.6	0.98
Air	11	0.23 ± 0.02	3.0	0.98

[a] Gas is purged in the reaction prior and during irradiation.
[b] $[PA]_0 = 38\ \mu mol/L$; $[TiO_2] = 0.1\ g/L$; $\lambda = 350\ nm$.

degradation kinetics as a function of solution pH and the results are summarized in Table 1. Solution pH can have a dramatic effect on the adsorption properties of TiO_2, esp. surface charge and aggregation. While higher adsorption of the negatively charged substrates (like PA) would be expected to increase as the surface of the TiO_2 becomes more positively charged (under acidic pH) we observed the maximum adsorption at almost neutral conditions. The rate and extent of TiO_2 aggregation can be dramatically influenced by the pH, ionic strength, and composition of the suspension. A recent report indicates the surface areas decrease under acid pH [40]. The reaction rates under acidic are modestly slower than at neutral conditions. When aggregation increases the surface area of TiO_2 decreases which could lead to lower observed adsorption and modestly slower degradation under acidic conditions. Although the adsorption was lower at pH 9 compared to acidic and neutral conditions, the increased anionic character of PA at pH 9 may enhance its reactivity towards hydroxyl radical, an electrophilic species. The observed decrease in degradation observed at pH = 11 under our conditions is attributed to a dominating effect of the electrostatic repulsion between the highly negatively charged surface of the TiO_2 and negatively charged PA.

3.5. Scavenging experiments for reactive oxygen species

TiO_2 PCO involves a complex interdependent series of reaction processes and a number of reactive oxygen species (ROS). In an attempt to assess the reaction processes and the roles of individual ROS, it is instructive to briefly discuss the sequence of events initiated during TiO_2 photocatalysis. Upon absorption of a photon an electron from the conduction band is promoted to the valence band creating an electron (e_{CB}^-)/hole (h_{VB}^+) pair (Eq. (4)).

$$TiO_2 + h\nu \rightarrow e_{CB}^- + h_{VB}^+ \quad (4)$$

In the absence of electron or hole trap, recombination of the e_{CB}^-/h_{VB}^+ pair occurs. Oxygen can act as an e_{CB}^- trap leading to superoxide anion radical (Eq. (5)), while extending the lifetime of the h_{VB}^+, thus promoting oxidation processes. In aqueous media, the h_{VB}^+ is trapped by surface hydroxyl groups to form surface bound •OH groups as illustrated in Eqs. (6) and (7).

$$e^-_{CB} + O_{2abs} \rightarrow O_2^{-\bullet}{}_{abs} \quad (5)$$

$$h^+_{VB} + Ti^{IV} - OH \rightarrow Ti^{IV} - OH^\bullet \quad (6)$$

$$h^+_{VB} + H_2O_{abs} \rightarrow {}^\bullet OH_{abs} + H^+ \quad (7)$$

while superoxide anion radical, $O_2^{-\bullet}$, and hydroxyl radical, •OH, are formed, •OH is generally believed to play the primary role in promoting oxidation during the TiO_2 photocatalysis [35]. Scavengers were employed to probe the roles of $O_2^{-\bullet}$ and •OH during the PA degradation process.

The results presented earlier demonstrate O_2 plays a key role in TiO_2 photocatalytic degradation of PA. Oxygen is critical as an electron scavenger to inhibit recombination of the electron/hole pair, thus promoting oxidative processes such as the formation

of hydroxyl radical. As a result of this process $O_2^{-\bullet}$ is produced, which can also lead to oxidation pathways. Superoxide anion radical has the potential to react directly by oxidative pathways, it can also produce singlet oxygen or decompose to H_2O_2, which is transformed to hydroxyl radical during TiO_2 photocatalysis. The addition of superoxide dismutase (SOD) to solution, which is an effective $O_2^{-\bullet}$ scavenger (Eq. (8)) [37], showed no effect on TiO_2 photocatalytic degradation of PA under our experimental conditions.

$$SOD_{red} + {}^{\bullet}O_2^- + 2H+ \rightarrow SOD + H_2O_2, \quad k = 2.0 \times 109\,M^{-1}\,s^{-1} \quad (8)$$

tert-Butyl alcohol readily reacts with •OH as illustrated by Eq. (9) [37,41]. Inhibition of the TiO_2 photocatalytic oxidation of methylated arsenic acids is observed upon addition *tert*-butyl alcohol [28,37]:

$$^{\bullet}OH + t\text{-BuOH} \rightarrow H_2O + {}^{\bullet}CH_2C(CH_3)_2OH, \quad k = 6.0 \times 10^8\,M^{-1}\,s^{-1} \quad (9)$$

The 1st order rate constant for TiO_2 photocatalyzed degradation of PA decreased by 67% from $0.36 \pm 0.04\,min^{-1}$ to $0.12 \pm 0.02\,min^{-1}$ in the presence of 5 vol% *t*-BuOH. While hydroxyl radical mediated processes can be completely inhibited in the presence of excess *t*-BuOH, modest degradation of PA is still observed. Since TiO_2 photocatalysis typically involves reactions at or near the surface, the adsorption properties of the substrates, *t*-BuOH and PA, can have a pronounced influence on the competition for the surface generated hydroxyl radicals. The target compound, PA, is at much lower concentrations than the scavenger, *t*-BuOH, but due to its stronger adsorption properties (localization near the production of oxidant), degradation still occurs.

The formation of singlet oxygen during TiO_2 photocatalysis has been recently reported [42]. Azide has been used as both a singlet oxygen and hydroxyl radical scavenger, represented by Eqs. (10) and (11) [37]. Addition of azide during photocatalysis decreases the degradation rate of PA to a rate of $0.17 \pm 0.03\,min^{-1}$.

$$^{\bullet}OH + N_3^- \rightarrow {}^{\bullet}N_3 + OH^-, \quad k = 1.0 \times 10^{10}\,M^{-1}\,s^{-1} \quad (10)$$

$$O^1 + N_3^- \rightarrow {}^{\bullet}N_3 + O_2^{\bullet -}, \quad k = 2.0 \times 10^9\,M^{-1}\,s^{-1} \quad (11)$$

Strong inhibition of the process by *t*-BuOH and azide provide convincing evidence for the participation of •OH in the oxidation of PA. Modest differences in the level of inhibition between the hydroxyl radical scavengers may be related to adsorption properties and/or slightly differences in the experimental conditions [43]. If singlet oxygen played a significant role in the degradation processes the level of inhibition by azide is expected to be greater than that observed for *t*-BuOH which only inhibits hydroxyl radical mediated processes. It does not appear that singlet oxygen plays a significant role under our experimental conditions.

Photoexcitation of TiO_2 leads to the formation of a hole, which can react with adsorbed H_2O or –TiOH, to yield hydroxyl radical on the surface of TiO_2. Formic acid has been used as hole scavenger during TiO_2 photocatalysis, Eq. (12). The hole is consumed by HCO_2^-, which can eliminate or intercept the generation of hydroxyl radical on TiO_2 [44]. Formic acid under neutral and acidic conditions is strongly adsorbed onto the surface of TiO_2. Upon addition of formic acid (0.5 g/L) to the solution the degradation rate of PA is almost completely inhibited ($k = 0.01 \pm 0.01\,min^{-1}$).

$$2\,h^+ + 2HCO_2^- \rightarrow CO_2 + 2H^+ \quad (12)$$

The results for the different scavengers are summarized in Fig. 5. Among the scavengers employed, formic acid leads to almost complete inhibition of the PA degradation, *t*-BuOH and N_3^- lead to >50% decrease in degradation rate. The competitive adsorption of formic acid with PA results in more effective inhibition of h_{VB}^+ and/or •OH compared to less strongly adsorbed scavengers, *t*-BuOH and N_3^-.

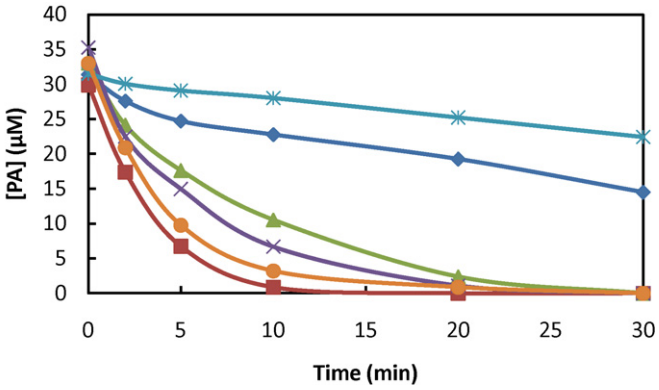

Fig. 5. Time profiles of PA degradation in the TiO_2 suspension with various scavengers. $[PA]_0 = 38\,\mu mol/L$; $[TiO_2] = 0.1\,g/L$; $\lambda = 350\,nm$; air-saturated except argon-saturated (◆ argon-saturated; ■ air-saturated; ● with 4000 U/mL SOD; ▲ with 5 vol% t-BuOH; ✕ with 0.2 g/L N_3^-; ✱ with 0.5 g/L formic acid).

The degradation of PA decreases in the presence of •OH and hole scavengers. Hydroxyl radical also plays an important role in the TiO_2 photocatalytic degradation of MMA and DMA to arsenate, and arsenite to arsenate [28,37,20,21].

3.6. Product studies

Product studies were carried out to elucidate the reaction pathways involved in the TiO_2 photocatalytic degradation of PA. Under

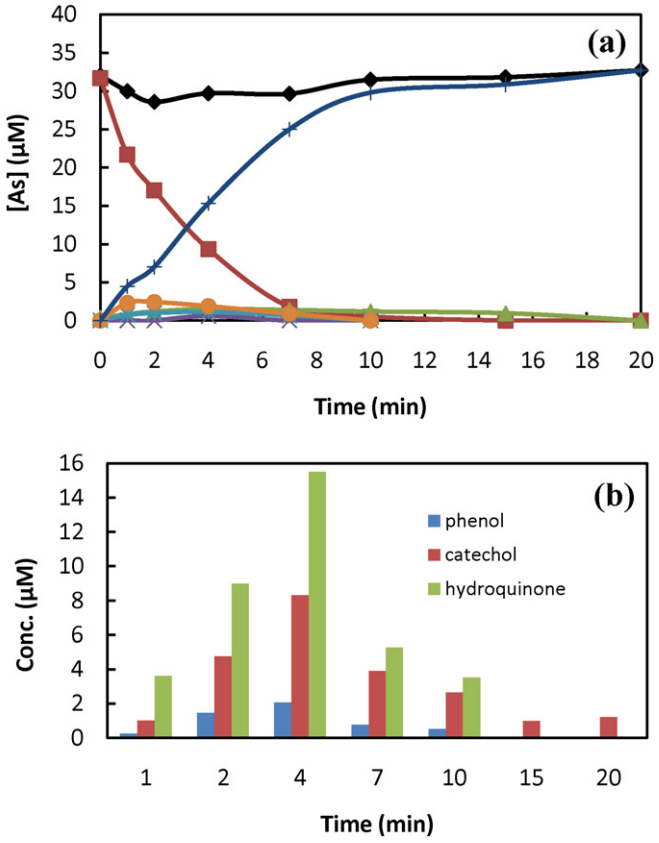

Fig. 6. (a) Relative concentrations of arsenic species in the solution during the TiO_2 photocatalytic degradation (♦ total As; ■ PA; ▲ As(III); ✕ 2-OH-PA; ✱ 4-OH-PA; ● DiOH-PA, dihydroxylated phenylarsonic acid; + As(V)). (b) Relative concentrations of organic species in the solution $[PA]_0 = 38\,\mu mol/L$; $[TiO_2] = 0.1\,g/L$; air-saturated; $\lambda = 350\,nm$.

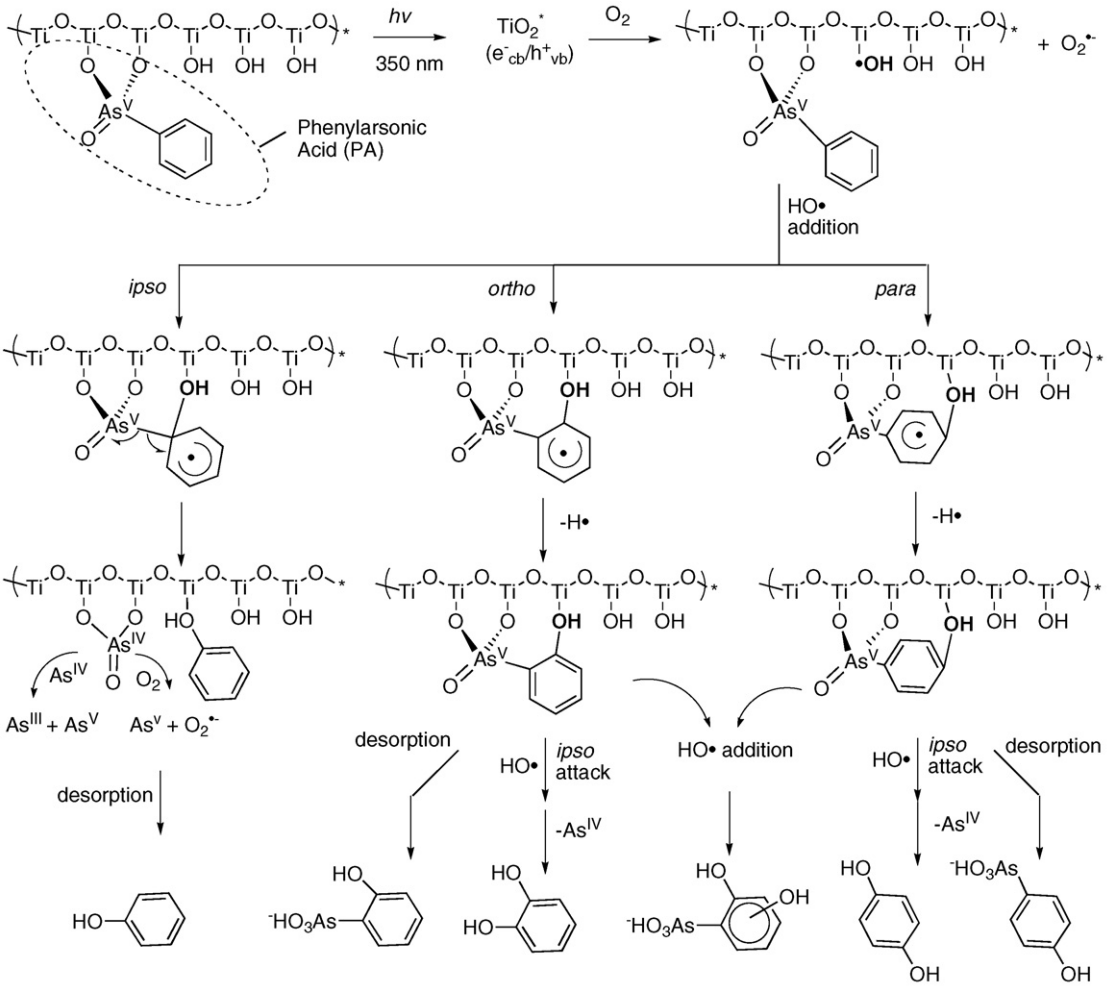

Fig. 7. Proposed surface mediated mechanism of TiO_2 photocatalytic degradation of PA.

homogeneous conditions, •OH reacts with PA via hydroxylation of the aromatic ring leading to phenolic products and inorganic arsenic species [30]. The final arsenic species produced during TiO_2 photocatalytic degradation of PA is arsenate. The mass balance for total arsenic throughout the degradation process is 80–90% because of adsorption on TiO_2. HPLC-ICP-MS analyses and comparison of chromatographic behavior with authentic samples was used to assign the identity of a number of the reaction products. Details of the analytical methods used for product identification are included in Section 2. Monohydroxylated and dihydroxylated phenylarsonic acids are intermediate products present at relatively low concentrations (<10%) during TiO_2 photocatalysis as illustrated in Fig. 6(a). Computational and product studies suggest •OH preferentially adds to the *ortho*- and *para*-positions of PA, yielding 2- and 4-hydroxyl adducts as the major initial products during radiolysis (homogeneous conditions) [30]. In contrast, phenol, catechol and hydroquinone are major degradation products from TiO_2 PCO of PA (heterogeneous conditions) confirmed by GC analyses of a methylene chloride extract of the reaction solution. The distribution of phenolic products is illustrated in Fig. 6(b). The dihydroxylated products, catechol (*ortho*-isomer) and hydroquinone (*para*-isomer), are major products, but we were not able to detect resorcinol, the *meta*-isomer. The observed phenolic products could also be the result of direct oxidation via h_{VB}^+, but *ipso*-addition of H_2O to the corresponding radical cation is not expected to yield the predominant observed products. The presence of phenols and inorganic arsenite and arsenate in the solution requires the cleavage of the arsenic-carbon bond in the PA molecule. The concentration of As(III) is low in solution and arsenate is the final product for the PA degradation.

The major observed products during TiO_2 PCO of PA are phenol, catechol and hydroquinone accounting for ~70% of the organic reaction products at a treatment time of 4 min, while only low levels of phenol were detected under radiolytic treatment [30]. As(III) is not observed during TiO_2 PCO of methylated species [28] thus cleavage of arsenic-carbon bond does not appear to involve the same type of cleavage pathway as observed for PA.

The strong adsorption of PA and hydroxylated PA to the TiO_2 surface where hydroxyl radicals are localized will enhance the probability for dihydroxylation. Preferential formation of the *ortho*- and *para*-dihydroxylated products is indicative of •OH mediated oxidation. The dihydroxylated products could be formed from reactions of phenol with hydroxyl radical or the result of dihydroxylation of PA followed by cleavage of the carbon-arsenic bond. The formation of catechol and hydroquinone initially and throughout the degradation processes suggest that arsenic bond cleavage follows dihydroxylation. While benzenetriols can be generated during the photocatalytic oxidation of substrates with benzene rings we did not observe such products by GC analyses. Successive •OH attack of the aromatic ring leads to carbonyl compounds, which can be mineralized to carbon dioxide and water [45].

3.7. Mechanism of TiO_2 photocatalytic degradation of PA

The degradation of most organic compounds on TiO_2 is typically initiated by an oxidative path (hole transfer or •OH radical reaction) [46]. The results of our scavenger experiments presented earlier clearly indicate hydroxyl radical plays a major role in the TiO_2 PCO of PA. Comparison of the results for arsenite, methylated arsenic species and PA demonstrate distinct differences among the reaction mechanisms for TiO_2 PCO of arsenite, methylated arsenic and phenylarsenic species. The mechanism for TiO_2 PCO of inorganic arsenite As(III) occurs by oxidation of the arsenic atom [20,21], while methylated arsenic species appear to react by hydrogen abstraction [30]. As(III) is observed during hydroxyl mediated oxidation of PA, but there is no report of the formation of As(III) during hydroxyl radical mediated oxidation of the corresponding methylated arsenic species [30,37].

Addition of •OH to the aromatic ring of PA can occur at four different positions, *ortho*, *para*, *meta*, and *ipso*. Addition at *ortho*-, *meta*- or *para*-position would yield the corresponding monohydroxylated PA derivatives. While *ortho*- and *para*-isomers are observed products, we were not able to confirm the formation of the *meta*-isomer. We attribute the selective formation of the *ortho*- and *para*-hydroxyl PAs to the electronic directing effect of the arsenate group in the parent compound. Under homogeneous conditions (radiolysis), hydroxyl radical leads to hydroxylation preferably at the *ortho*- and *para*-position leading to hydroxyl-PA products as the predominant pathway [30], however TiO_2 PCO (heterogeneous conditions) appears to promote the formation of catechol and hydroquinone requiring addition of two hydroxyl groups with cleavage of the arsenic-carbon bond. The proposed surface mediated hydroxyl radical reactions are illustrated in Fig. 7. Following initial addition of hydroxyl radical to the aromatic ring of PA, addition of a second hydroxyl group could yield a dihydroxylated PA adduct. Hydroxyl radical could also add to the *ipso*-position (carbon at position of As attachment) to yield a radical intermediate which upon collapse via arsenic-carbon bond homolysis can lead to the observed products, catechol and hydroquinone. The latter reaction appears to be the predominant reaction pathway during TiO_2 PCO based on the observed product distribution. The adsorption of the arsenic group onto the TiO_2 in the monohydroxylated PA adducts may weaken the arsenic-carbon bond making it more susceptible to elimination compared to radiolysis conditions where catechol and hydroquione were not the predominant products. As(IV), a by-product of the homolytic arsenic-carbon bond cleavage, readily disproportionates to yield 1:1 ratio of As(III) and As(V) [29], leading to the As(III) observed during TiO_2 photocatalytic degradation of PA. As(III) is oxidized to arsenate by molecular oxygen, •OH or h_{VB}^+, and converted to As(V) [20,47].

4. Conclusion

In summary, TiO_2 photocatalytic degradation of phenylarsonic acid leads to mineralization to As(V). While inorganic arsenic species are generally considered to be more toxic than organoarsenic species, there are well-established methods for the removal of arsenate from water. The degradation kinetics for PA is nicely modeled by simple kinetic processes and indicates the reactions occur at or near the surface of TiO_2. The adsorption and degradation of PA during TiO_2 photocatalysis parallel the electrostatic interactions between the TiO_2 surface and PA as a function of solution pH. Experiments conducted in the presence of hydroxyl radical, superoxide anion radical, singlet oxygen and hole scavengers indicate that hydroxyl radical plays a key role during TiO_2 photocatalysis of PA. The reaction pathway observed for PA is different than those reported for inorganic arsenic and methylated arsenic species. Different product distributions are observed for radiolysis and TiO_2 PCO of PA. A surface mediated reaction mechanism is proposed to explain the formation of the observed reaction products. The TiO_2 surface appears to play an important role in the partitioning of the reaction pathways leading to the formation of As(V). TiO_2 photocatalysis can be effectively employed to treat and remove the organoarsenic species from contaminated water.

Acknowledgments

K.E.O. gratefully acknowledges support from the NIH/NIEHS (Grant No. S11ES1118). We thank the reviewers for valuable insight and suggestions.

References

[1] C.K. Jain, I. Ali, Water Res. 34 (2000) 4304–4312.
[2] A.H. Smith, P.A. Lopipero, M.N. Bates, C.M. Steinmaus, Science 296 (2002) 2145–2146.
[3] D.C. Adriano, Trace Elements in the Terrestrial Environment, Springer, New York, 2001.
[4] O.S. Thirunavukkarasu, T. Viraraghavan, K.S. Subramanian, Water SA 29 (2003) 161–170.
[5] J. Hlavay, K.J. Polyak, Colloids Interface Sci. 284 (2005) 71–77.
[6] A.H. Welch, M.S. Lico, J.L. Hughes, Ground Water 26 (1988) 333–347.
[7] http://www.atsdr.cdc.gov/toxprofiles/tp2-c6.pdf.
[8] B.P. Jackson, P.M. Bertsch, Environ. Sci. Technol. 35 (2001) 4868–4873.
[9] J.R. Garbarino, A.J. Bednar, D.W. Rutherford, R.S. Beyer, R.L. Wershaw, Environ. Sci. Technol. 37 (2003) 1509–1514.
[10] B.M. Onken, L.R. Hossner, Soil Sci. Soc. Am. J. 60 (1996) 1385–1392.
[11] A.R. Marin, S.R. Pezeshki, P.H. Masschelen, H.S. Choi, J. Plant Nutr. 16 (1993) 865–880.
[12] P.A. Moore, T.C. Daniel, J.T. Gilmour, B.R. Shreve, D.R. Edwards, B.H. Wood, J. Environ. Qual. 27 (1998) 92–99.
[13] A.J. Bednar, J.R. Garbarino, I. Ferrer, D.W. Rutherford, R.L. Wershaw, J.F. Ranville, T.R. Wildeman, Sci. Total Environ. 302 (2003) 237–245.
[14] H. Castlehouse, C. Smith, A. Raab, C. Deacon, A.A. Meharg, J. Feldmann, Environ. Sci. Technol. 37 (2003) 951–957.
[15] I.N. Nartyanov, E.N. Savinov, J. Photochem. Photobiol. A: Chem. 134 (2000) 219–226.
[16] U.I. Gaya, A.H. Abdullah, J. Photochem. Photobiol. C: Photochem. Rev. 9 (2008) 1–12.
[17] P.K. Dutta, S.O. Pehkonen, V.K. Sharma, A.K. Ray, Environ. Sci. Technol. 39 (2005) 1827–1834.
[18] M.A. Fox, M.T. Dulay, Chem. Rev. 93 (2003) 341–357.
[19] A.L. Linsebigler, G. Lu, J.T. Yates, Chem. Rev. 95 (1995) 735–758.
[20] T. Xu, P.V. Kamat, K.E. O'Shea, J. Phys. Chem. A 109 (2005) 9070–9075.
[21] S. Yoon, S. Oh, J.E. Yang, J.H. Lee, M. Lee, S. Yu, D. Par, Environ. Sci. Technol. 43 (2009) 864–869.
[22] J. Ryu, W. Choi, Environ. Sci. Technol. 38 (2004) 2928–2933.
[23] W.H. Leng, X.F. Cheng, J.Q. Zhang, C.N. Cao, Environ. Sci. Technol. 41 (2007) 6311–6312.
[24] J. Ryu, W. Choi, Environ. Sci. Technol. 41 (2007) 6313–6314.
[25] S. Yoon, J.H. Lee, Environ. Sci. Technol. 39 (2005) 9695–9701.
[26] M. Bissen, M.M. Vieillard-Baron, A.J. Schindelin, F.H. Frimmel, Chemosphere 44 (2001) 751–757.
[27] H. Lee, W. Chow, Environ. Sci. Technol. 36 (2002) 3872–3878.
[28] T. Xu, Y. Cai, K.E. O'Shea, Environ. Sci. Technol. 41 (2007) 5471–5477.
[29] U.K. Klaning, B.H.J. Bieski, K. Sehested, Inorg. Chem. 28 (1998) 2717–2724.
[30] T. Xu, P.V. Kamat, S. Joshi, A.M. Mebel, Y. Cai, K.E. O'Shea, J. Phys. Chem. A 11 (2007) 7819–7824.
[31] J. Calvert, J.N. Pitts, Photochemistry, Wiley, New York, 1966.
[32] P.K. Dutta, A.K. Ray, V.K. Sharma, F.J. Millero, J. Colloid Interface Sci. 278 (2004) 270–275.
[33] R. Mueller, H.K. Kammler, K. Wegner, S.E. Pratsinis, Langmuir 19 (2003) 160–165.
[34] K.E. O'Shea, E. Pernas, J. Saiers, Langmuir 15 (1999) 2071–2076.
[35] C.S. Turchi, D.F. Ollis, J. Catal. 122 (1999) 178–192.
[36] H. Tada, Langmuir 12 (1996) 966–971.
[37] Z. Xu, C. Jing, F. Li, X. Meng, Environ. Sci. Technol. 42 (2008) 2349–2354.
[38] C. Jiang, X. Meng, S. Liu, S. Baidas, R. Patraju, C. Christodoulatos, G.P. Korfiatis, J. Colloid Interface Sci. 290 (2005) 14–21.
[39] S. Parra, J. Oliverob, C. Pulgarin, Appl. Catal. B: Environ. 36 (2002) 75–85.
[40] N. Mandzy, E. Grulke, T. Druffel, Powder Technol. 160 (2005) 121–126.
[41] B. Subramanian, Q. Yang, Q. Yang, A.P. Khodadoust, D.D. Dionysiou, J. Photochem. Photobiol. A: Chem. 192 (2007) 114–121.
[42] T. Daimon, Y. Nosaka, J. Phys. Chem. C 111 (2007) 4420–4424.

[43] H.J. Cha, O.K. Park, Y.H. Kim, H.G. Cha, Y.S. Kang, Int. J. Nanosci. 5 (2006) 795–801.
[44] V.N.H. Nguyen, D. Beydoun, R. Amal, J. Photochem. Photobiol. A: Chem. 171 (2005) 113–120.
[45] A. Sobczyński, L. Duczmal, W. Zmudziński, J. Mol. Catal. A Chem. 213 (2004) 225–230.
[46] M.R. Hoffmann, S.T. Martin, W. Choi, D.W. Bahnemann, Chem. Rev. 95 (1995) 69–96.
[47] P.M. Huang, D.W. Oscarson, W.K. Liaw, U.T. Hammer, Hydrobiologia 91–92 (1982) 315–322.